

# Thermophysical and Phase Properties of Polymer/Liquid Crystal Systems: Theoretical Aspects and Experimental Examples<sup>†</sup>

Réda Benmouna\* and Mustapha Benmouna

Department of Physics, Faculty of Sciences, University Aboubekr Belkaïd, Tlemcen BP119, Algeria

The thermophysical properties and phase behavior of polymer/liquid crystal systems are reviewed. These systems, often called polymer-dispersed liquid crystals (PDLCs), have a variety of applications encompassing electrically activated windows with controlled light transmission, display panels, fiber optics, and multiplexing devices for telecommunication systems. Most applications rely on specific electro-optical responses that in turn depend on the phase behavior and thermophysical properties in addition to the morphology and dimensions of the LC domains. This is why a detailed study of thermophysical properties is necessary to better comprehend the performance under practical conditions in applications. This paper reviews the theories used to understand these properties and gives some experimental examples used as tests for the theory. A biased selection of experimental studies already reported in the literature has been chosen as a basis for discussing the main features of the properties of polymer/liquid crystal composites and assessing the applicability of the models. These examples use a variety of polymers with different architectures, including acrylates, siloxanes, and thiolene monomers, together with LCs exhibiting different kinds of order.

## Introduction

Polymers and liquid crystal (LC) systems are interesting from different points of view involving theoretical modeling, experimental investigation, and practical applications. High-molecular-weight polymers usually consist of long flexible chains, while liquid crystals are small rigid molecules with orientation properties. Under certain conditions, these molecular species are chemically bound to form a new class of polymers known as side- or main-chain liquid crystal polymers. When they are simply mixed, they form yet another class, often called polymer-dispersed liquid crystals (PDLCs). Clearly, these systems combine the properties of polymers (with their diversity) and LCs (with a variety of phase transitions).<sup>1,2</sup> This paper reviews the thermophysical and phase properties of PDLCs essentially in terms of temperature and composition, focusing primarily on the aspects with which the authors have been involved directly or indirectly. An exhaustive review combining other properties of polymer/LC systems would be too broad and is beyond the scope of this paper.

PDLCs consist of films with a Swiss cheese morphology in which the LC molecules are confined in droplets. These droplets are randomly dispersed, and their size spans the range from micrometers to nanometers, depending on the materials used, the conditions of preparation, and the application needs. Micrometer-thick films are often used in switchable windows with electrically activated and controlled light transmission. When an electric field is applied, nematic domains usually align along the field direction, giving a transparent, weakly scattering system. Conventional flat-panel display devices are made of twisted nematic LCs, but these are expensive and use large quantities of LC. PDLCs are good substitutes for these devices with the advantages of being robust, highly performing, and cheaper. In addition, they are easily fabricated and cover large

areas with reflective displays that have a high efficiency and good contrast ratio. Multiplexing capabilities can also be obtained under certain conditions.<sup>3,4</sup>

This paper is organized as follows: The next section presents some theoretical aspects of the problem. The properties of isotropic mixtures of polymers and LCs are described on the basis of the Flory–Huggins lattice model.<sup>5</sup> These properties apply to initial solutions before polymerization (i.e., uncured monomer/LC systems) and to systems involving linear polymers. For cross-linked networks, chemical binding of chains limits their swelling capabilities and confers rubberlike behavior to the network, as modeled by Flory–Rehner theory.<sup>6</sup> The nematic order is described by Maier–Saupe theory, while the smectic-A order is introduced using McMillan theory.<sup>7,8</sup> Experimental examples are then given to illustrate the applicability of the theory. The list of examples is limited essentially to systems with which the authors have some familiarity. The last section gives a brief analysis of results that highlight major effects deduced from the confrontation of experiments and theory, followed by a conclusion.

## Theoretical Considerations

Different methods of describing the thermodynamic properties of polymer and LC systems have been reported in the literature. These are based essentially on the lattice model, but sometimes other approaches have been suggested, such as the equation of state model.<sup>9</sup> Ballauff and co-workers<sup>10–13</sup> applied the Flory lattice model to a variety of systems and observed qualitative agreement with experiments. They suggested that some quantitative discrepancies could be resolved by assuming a mass-fraction-dependent interaction parameter. They observed that polymers underwent an abrupt size reduction at the isotropic to nematic transition with dimensions hardly exceeding those of the dry state.

Kyu and co-workers<sup>14–16</sup> performed an extensive investigation of the phase behavior of PDLCs involving linear polymers,

<sup>†</sup> Part of the “Josef M. G. Barthel Festschrift”.

\* Corresponding author. E-mail: redabenmouna@yahoo.com.

cross-linked networks, or side-chain liquid crystal polymers. They examined nematic and smectic-A systems as well as their mixtures. Similar approaches to these problems were also reported by Benmouna and co-workers.<sup>17–19</sup> The present section is a brief discussion of these methods.

**The Isotropic State.** Most theoretical models used to establish the phase diagrams and discuss the thermophysical properties of polymer/LC mixtures were developed starting from an expression of free energy. We first discuss the case of isotropic mixing using the Flory–Huggins model for linear molecules and the Flory–Rehner theory for networks exhibiting rubberlike elasticity behavior.

For linear molecules, the free-energy density  $f_{\text{iso}}^5$  is given by

$$\frac{f_{\text{iso}}}{k_{\text{B}}T} = \frac{\varphi_1}{N_1} \ln \varphi_1 + \frac{\varphi_2}{N_2} \ln \varphi_2 + \chi \varphi_1 \varphi_2 \quad (1)$$

where  $\chi$  is the Flory–Huggins interaction parameter,  $k_{\text{B}}$  is Boltzmann's constant,  $T$  is the absolute temperature, and subscripts 1 and 2 refer to the LC and substrate (polymer or monomer), respectively. The numbers of repeat units are  $N_1$  for the LC and  $N_2$  for the substrate. Typically,  $N_1 = 1$  while  $N_2$  depends on chain dimension. The volume fractions of LC ( $\varphi_1$ ) and polymer or monomer ( $\varphi_2$ ) are defined as

$$\varphi_1 = \frac{n_1 N_1 v_0}{V_{\text{T}}} \quad \varphi_2 = \frac{n_2 N_2 v_0}{V_{\text{T}}} \quad (2)$$

in which  $v_0$  is a reference volume (e.g., the volume of a lattice site) that is assumed to be the same for the LC and monomer,  $n_1$  and  $n_2$  are the numbers of molecules, and the total volume  $V_{\text{T}}$  is given by

$$V_{\text{T}} = (n_1 N_1 + n_2 N_2) v_0 = n_{\text{T}} v_0$$

in which  $n_{\text{T}}$  is the total number of sites in the lattice. Miscibility behavior of the mixture is described in the temperature composition frame according to the values of  $N_1$ ,  $N_2$ , and  $\chi$ . For monomer systems, the phase diagram exhibits a standard form since  $N_1$  and  $N_2$  are close to each other and  $\chi$  is weak. Dissymmetry is enhanced with increasing  $N_2$ , accompanied by a reduced miscibility due to entropy loss and energy gain.

In the case of cross-linked networks, the free energy shows an elastic contribution in addition to the mixing term. The Flory–Rehner theory of rubber elasticity<sup>6</sup> gives  $f_{\text{iso}}$  as

$$\frac{f_{\text{iso}}}{k_{\text{B}}T} = \frac{3\alpha\varphi_0^{2/3}}{2N_{\text{c}}}(\varphi_0^{1/3} - \varphi_2) + \frac{\beta\varphi_2}{N_{\text{c}}} \ln \varphi_2 + \frac{\varphi_1}{N_1} \ln \varphi_1 + \chi\varphi_1\varphi_2 \quad (3)$$

in which  $N_{\text{c}}$  represents the number of repeat units between consecutive cross-links and  $\varphi_0$  is the polymer volume fraction prior to cross-linking. The parameters  $\alpha$  and  $\beta$  are model-dependent. According to James and Guth,<sup>20</sup> these parameters should be constant ( $\alpha = 1$  and  $\beta = 1$ ).<sup>21,22</sup> Flory<sup>5</sup> suggested that  $\beta$  should be related to the monomer functionality  $f$  as  $\beta = 2/f$ , while Petrovic et al.<sup>22</sup> proposed that both  $\alpha$  and  $\beta$  are composition-dependent and should be expressed as  $\alpha = (f - 2 + 2\varphi_2)/f$  and  $\beta = 2\varphi_2/f$ . In this theory, the Flory model is recovered in the bulk state with  $\varphi_2 = 1$ , while the James–Guth model is obtained in the limit of  $\varphi_2 = 1$  and  $f = 2$ . In order to improve the accordance between theory and experiment, the  $\chi$  parameter is often assumed to depend on temperature and mass fraction. We will come back to this point later.

The chemical potential of each component is calculated by differentiating the total free energy  $F = n_{\text{T}}f$  with respect to the number of molecules  $n_1$  or  $n_2$ . More explicitly, we have  $\mu_1 =$

$(\partial F/\partial n_1)_{n_2, T}$  and  $\mu_2 = (\partial F/\partial n_2)_{n_1, T}$ . It is convenient to express these derivatives in terms of volume fractions instead of numbers of molecules as

$$\mu_1 = N_1 \left[ f - \varphi_2 \frac{\partial F}{\partial \varphi_2} \right] \quad \mu_2 = N_2 \left[ f - \varphi_1 \frac{\partial F}{\partial \varphi_1} \right] \quad (4)$$

These results are valid for monomer systems, linear polymers with high molecular weights (i.e., large values of  $N_2$ ), and cross-linked networks [i.e.,  $\mu_2(\text{network}) = f - \varphi_1(\partial F/\partial \varphi_1)$ ]. In a miscibility gap, the chemical potentials for each component in coexisting phases are equal, and the compositions are found by solving the set of equations  $\mu_1' = \mu_1''$  and  $\mu_2' = \mu_2''$ , where primes refer to the phases in equilibrium. Hence, the bimodal curve is simply obtained by writing that  $f - \varphi_2(\partial f/\partial \varphi_2)$  and  $(\partial f/\partial \varphi_2)$  are equal in the two phases. The spinodal curve is obtained from the second derivative of the free energy as  $(\partial^2 f/\partial \varphi_2^2) = 0$ , while the critical point is directly inferred by setting the second and third derivatives of the free energy equal to zero. For a linear polymer of size  $N_2$ , the critical-point coordinates  $T_{\text{c}}$  and  $\varphi_{\text{c}}$  are

$$T_{\text{c}} = 2B \left[ \frac{1}{N_1 \varphi_1} + \frac{1}{N_2 \varphi_2} - 2A \right]^{-1} \quad \varphi_{\text{c}} = \frac{\sqrt{N_2}}{\sqrt{N_1} + \sqrt{N_2}} \quad (5)$$

where the constants  $A$  and  $B$  define the temperature dependence of  $\chi$ , which is given by  $\chi = A + B/T$ .

**The Nematic Order.** The total free energy is the sum of isotropic and nematic contributions. The latter is modeled according to Maier–Saupe theory<sup>7</sup> as follows:

$$\frac{f_{\text{nematic}}}{k_{\text{B}}T} = \frac{\varphi_1}{N_1} \left[ -\ln Z + \frac{1}{2} \nu \varphi_1 S^2 \right] \quad (6)$$

where the first term on the right-hand side expresses the loss of entropy due to nematic order and the second term is the nematic interaction. In the first term, the corresponding partition function  $Z$  is given by

$$Z = \int e^{-U(\theta)/k_{\text{B}}T} d(\cos \theta) \quad (7)$$

where  $\theta$  represents the angle between an LC molecule and the director and  $U(\theta)$  is the nematic interaction potential:

$$\frac{U(\theta)}{k_{\text{B}}T} = -\frac{m_{\text{n}}}{2} [3 \cos^2 \theta - 1] \quad (8)$$

In eq 8, the mean-field parameter  $m_{\text{n}}$  has been introduced to describe the strength of the interaction. Minimization of the free energy yields  $m_{\text{n}} = \nu \varphi_1 S$ , where  $\nu$  is the Maier–Saupe quadrupole interaction parameter, given by  $\nu = 4.54 \cdot T_{\text{NI}}/T$ , in which  $T_{\text{NI}}$  is the temperature of the isotropic to nematic transition. The order parameter  $S$  is related to the first Legendre polynomial as

$$S = \frac{1}{2} \langle 3 \cos^2 \theta - 1 \rangle \quad (9)$$

where the symbol  $\langle \dots \rangle$  represents an angular average with respect to the distribution function  $\Psi(\theta)$ :

$$\Psi(\theta) = Z^{-1} \exp[-U(\theta)/k_{\text{B}}T]$$

It is worth noting that the order parameter can be obtained using the expression  $S = (\partial \ln Z/\partial m_{\text{n}})$ .

**The Smectic-A Order.** Smectic-A is a directional order with a succession of layers having an interlayer spacing  $d$ . The free-energy contribution of these layers contains entropic and interaction terms that can be modeled according to McMillan theory as<sup>8</sup>

$$\frac{f_{\text{smectic}}}{k_{\text{B}}T} = \frac{\varphi_1}{N_1} \left[ -\ln Z + \frac{1}{2} \nu \varphi_1 (S^2 + \zeta \sigma^2) \right] \quad (10)$$

Assuming that layers are stacked along the  $z$  direction, one can define the order parameter  $\sigma$  as

$$\sigma = \frac{1}{2} \left\langle (3 \cos^2 \theta - 1) \cos \frac{2\pi z}{d} \right\rangle \quad (11)$$

The parameter  $\zeta$  depends on the ratio  $T_{\text{SN}}/T_{\text{NI}}$ , where  $T_{\text{SN}}$  is the temperature of the nematic to smectic transition. According to McMillan, when  $\zeta < 0.98$ , one should have the sequence of transitions isotropic  $\rightarrow$  nematic  $\rightarrow$  smectic, while for  $\zeta \geq 0.98$ , a direct transition from isotropic to smectic should occur. The partition function in the smectic-A order reads:

$$Z = \int d(\cos \theta) \int dz \exp \left[ \frac{m_{\text{n}}}{2} (3 \cos^2 \theta - 1) + \frac{m_{\text{s}}}{2} (3 \cos^2 \theta - 1) \cos \frac{2\pi z}{d} \right] \quad (12)$$

where minimization of the free energy shows that the mean-field parameters  $m_{\text{n}}$  and  $m_{\text{s}}$  are given by  $m_{\text{n}} = \nu S \varphi_1$  and  $m_{\text{s}} = \nu \zeta \sigma \varphi_1$ . For  $\zeta < 0.98$  and  $T < T_{\text{SN}}$ , the order parameter  $\sigma$  is found to decrease with the LC volume fraction, and at  $\varphi_{\text{SN}} = T_{\text{SN}}/T$ , it drops abruptly to zero. At the same time, the nematic order parameter  $S$  decreases sharply but remains finite until the LC volume fraction reaches  $\varphi_{\text{NI}} = T_{\text{NI}}/T$ , where  $S$  vanishes and the system becomes isotropic.

**The Case of Binary Nematogen Mixtures.** These mixtures exhibit a variety of interesting phases depending on the intrinsic properties of the individual components and their coupling. A simple example is given by mixtures of side-chain LC polymers and low-molecular-weight LCs in which the side-chain nematogen is grafted to the polymer backbone via flexible spacers. A large miscibility is expected if the nematogens have similar chemical structures.<sup>23,24</sup> As the length and flexibility of the spacers increase, the degree of coupling between the polymer backbone and the grafted LCs weakens, approaching the properties of simple LC mixtures. A more quantitative view of these features can be reached by considering the free energy in the ordered state, which is given by

$$\frac{f_{\text{nematic}}}{k_{\text{B}}T} = -\varphi_1 \ln Z_1 - \varphi_2 \ln Z_2 + \frac{1}{2} [\nu_{11} \varphi_1^2 S_1^2 + \nu_{22} \varphi_2^2 S_2^2 + 2\nu_{12} \varphi_1 \varphi_2 S_1 S_2] \quad (13)$$

where  $\nu_{ij}$  represent quadruple interaction parameters. The diagonal terms are given by  $\nu_{ii} = 4.54 \cdot T_{\text{NI},i}/T$  ( $i = 1, 2$ ), and the cross term is defined as  $\nu_{12}^2 = c \nu_{11} \nu_{22}$ , where the coupling constant  $c$  is related to the length and flexibility of the spacer: if  $c > 1$ , coupling is strong, and if  $c < 1$ , it is weak. The corresponding partition functions and order parameters are defined as before, i.e.,  $Z_i = \int d(\cos \theta_i) \exp[m_i(3 \cos^2 \theta_i - 1)/2]$  and  $S_i = (\partial \ln Z_i / \partial m_i)$  ( $i = 1, 2$ ), while the mean-field parameters  $m_i$  are obtained from minimization of the free energy as  $m_1 = \nu_{11} \varphi_1 S_1 + \nu_{12} \varphi_2 S_2$  and  $m_2 = \nu_{22} \varphi_2 S_2 + \nu_{12} \varphi_1 S_1$ .

In the weak-coupling limit ( $c < 1$ ), the order parameters show a minimum with respect to the LC volume fraction  $\varphi_1$ , and for intermediate coupling ( $c \approx 1$ ), they follow similar trends that

decrease with respect to  $\varphi_1$ . For strong coupling ( $c > 1$ ),  $S_1$  and  $S_2$  are quite large and change slightly with  $\varphi_1$  at low temperature, but at high temperature, they show a maximum. Phase diagrams exhibit a peculiar teapot configuration with a variety of domains. For a system in which the polymer is the majority component, nematic ordering is driven by the side chain; otherwise, it is the low-molecular-weight LC that controls the phase behavior. Interestingly, in the strong coupling regime, the diagram becomes simple, and the nematogens show enhanced miscibility in spite of their differences. A large domain with a single nematic phase is possible, with a relatively narrow gap between a nematic phase and an isotropic phase at high temperatures. At low temperatures, a small gap of nematogens is observed. Kyu et al.<sup>25</sup> suggested that in the strong-coupling limit, a smectic phase should appear even when the individual LCs do not exhibit such higher ordering. Similar trends are found in the case of cross-linked polymers. However, the teapot configuration is no longer observed.

## Experimental Examples

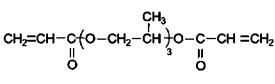
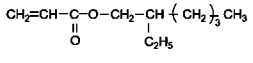
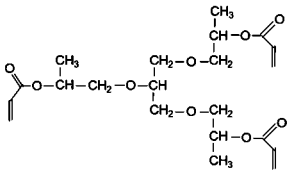
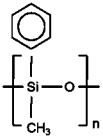
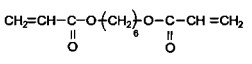
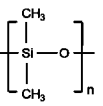
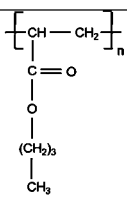
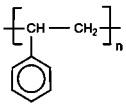
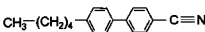
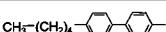
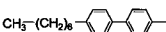
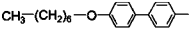
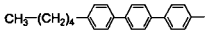
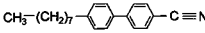
The results presented in this section are essentially adaptations from the cited references, unless otherwise specified. For this reason, some details have been omitted in favor of general tendencies that capture the main features of the thermal properties and phase behavior. A biased selection of examples is given, but the observations apply to a variety of other systems. Table 1 shows the structures of the monomers and LCs considered in this review. This is an arbitrary selection whose aim is to illustrate only major effects and tendencies found in polymer/LC systems and PDLCs in particular. Except in the case of Norland Optical Adhesive 65, only curves found using modeling calculations will be shown with no explicit data points. Again, this has been done in order to illustrate trends without giving particular attention to the exact numbers, unless explicitly specified otherwise.

**Polystyrene.** The first example describes the phase behavior and thermophysical properties of linear polystyrene (PS) and 4-cyano-4'-*n*-octylbiphenyl (8CB). This example illustrates the effects of the polymer molecular weight and the smectic order of the LC. References 26 and 27 describe how a combination of solvent-induced phase separation (SIPS) and thermally induced phase separation (TIPS) was used to prepare the samples. To summarize the method, blends of polymer and LC at different compositions were dissolved in tetrahydrofuran (THF) at a mass fraction of 0.50 and then stirred mechanically for over 12 h. The phase diagrams were established by differential scanning calorimetry (DSC) and validated by polarizing optical microscopy (POM). All of the details of sample preparation and measuring devices are given in refs 26 and 27. Reference 28 reports a small-angle neutron scattering study of the same blend to characterize its structural properties.

The phase diagrams in Figure 1 are of the upper critical solution temperature (UCST) type.<sup>26,27</sup> The critical point conformed well with theoretical predictions, except in the case of the low-molecular-weight system, for which the diagram shows a distortion due to nematic order. The isotropic-liquid-like gap also was not observed in this case. Larger miscibility gaps appear with higher PS sizes, and clear isotropic  $\rightarrow$  nematic  $\rightarrow$  smectic  $\rightarrow$  crystalline sequences are found. The temperature range shown in this figure does not cover the last transition.

These sequences take place at the same temperatures regardless of the PS size, supporting the view that ordered phases are made of pure LC. Some tendency toward a decrease in  $T_{\text{NI}}$  is seen in the lower range of LC mass fraction, which could be

**Table 1. Chemical Structures of (a) Monomers and (b) Liquid Crystals Cited in the Experimental Examples<sup>a</sup>**

(a) Monomers	
<p>- <i>Acrylates</i></p>  <p>tripropylene glycol diacrylate (TPGDA)</p>	 <p>poly(ethylhexyl acrylate) (PEHA)</p>
 <p>glycol propyl triacrylate (GPTA)</p>	<p>- <i>Siloxanes</i></p>  <p>poly(methylphenylsiloxane) (PMPS)</p>
 <p>1,6-hexanediol diacrylate (HDDA)</p>	 <p>poly(dimethylsiloxane) (PDMS)</p>
 <p>poly(<i>n</i>-butyl acrylate)</p>	<p>- <i>Polystyrene</i></p>  <p>polystyrene (PS)</p>
(b) Liquid Crystals	
<p>- <i>Nematic LC</i></p> 	<p>4-cyano-4'-<i>n</i>-pentylbiphenyl (5CB)</p> <p><math>T_{KN} = 296 \text{ K}; T_{NI} = 308.3 \text{ K}</math></p>
<p>5CB:  51%</p> <p>7CB:  25%</p> <p>8OCB:  16%</p> <p>5CT:  8%</p>	<p>E7 mixture</p> <p><math>T_{NI} = 333 \text{ K}</math></p>
<p>- <i>Smectic LC</i></p> 	<p>4-cyano-4'-<i>n</i>-octylbiphenyl (8CB)</p> <p><math>T_{KS} = 294.5 \text{ K}; T_{SN} = 306.5 \text{ K};</math> <math>T_{NI} = 313.5 \text{ K}</math></p>

<sup>a</sup> Abbreviations:  $T_{NI}$ , nematic to isotropic transition temperature;  $T_{KN}$ , crystalline to nematic transition temperature;  $T_{KS}$ , crystalline to smectic-A transition temperature.

attributed to the proximity of the polymer glass transition temperature,  $T_g$ . We again stress the fact that these curves were calculated using the formalism above. They clearly show the trends characterizing the phase behavior of such blends. In the theory, it is more convenient to use volume fractions ( $\varphi$ ), but in the experimental diagrams, these have been transformed into mass fractions ( $w$ ).

DSC analysis gives direct access to important thermal events, in particular to  $T_g$  and the enthalpy changes at transitions. A

particular example of  $T_g$  as a function of LC mass fraction  $w(\text{LC})$  is shown in Figure 1d. This temperature is found to decrease first rapidly as a small amount of LC is added and then steadily from (383 to 303) K as the mass fraction of 8CB increases from zero (pure PS) to 0.30. Such a plasticizing effect has important consequences for the system performance, mechanical strength, and aging behavior. It implies that the amount of LC remaining in the polymer matrix ( $\alpha$ ) must be precisely evaluated. Figure 1e shows that  $\alpha$  increases substantially with  $w(\text{LC})$  because of the reduced miscibility and drop in  $T_g$ . The enthalpy exchanges at transitions are readily deduced from the peaks of DSC thermograms. The heat exchange at the smectic  $\rightarrow$  nematic transition is quite low in comparison with that for the nematic  $\rightarrow$  isotropic transition, as shown in Figure 1f. However, the intersection with the  $x$  axis consistently gives the same result.

These data show typical effects of the polymer size and the smectic-A ordering in the LC. They are useful for assessing the general tendencies of the phase behavior of similar systems and apprehending performance under practical conditions in applications. Polymer supports are required to fulfill certain conditions of mechanical strength, aging, optical clarity, and dielectric quality. They host the LC component according to the needs in terms of responses to variations of temperature, composition, and external activation due to electric or magnetic fields, shear stress, and other excitations. The knowledge of  $T_g$  is of primary importance, and dispersion of the LC in the polymer directly modifies its value. Therefore, its amount should be reduced as much as possible to improve the mechanical strength of the system together with its optical and dielectric properties. Heat exchange is related to major thermodynamic events such as phase separation and the miscibility limit of similar interacting species. For example  $\Delta H_{NI}$  becomes nonzero at a certain mass fraction of LC where the system develops a new ordered phase. Finally, the mean-field theories presented in Theoretical Considerations seem sufficient to describe the main features of these findings.

**Polysiloxanes.** Experimental studies involving linear polysiloxanes are reported in refs 29–31. They include both poly(dimethylsiloxane) (PDMS) and poly(methylphenylsiloxane) (PMPS) together with the LCs E7 and 4-cyano-4'-*n*-pentylbiphenyl (5CB). The same sample preparation protocol was used as in the case of PS. Blends of polymer and LC at given compositions were dissolved in a common solvent (THF) at  $w(\text{LC}) = 0.55$ , except for the system with the highest PDMS molecular mass, for which  $w(\text{LC}) = 0.70$ . The mixtures were then stirred mechanically for several hours, after which the THF was allowed to evaporate at ambient temperature. The phase diagrams were established by a combination of DSC and POM. Here we present a selected part of the reported results. Figure 2a–c shows the theoretical diagrams for PDMS and 5CB for different molecular masses. Results for a cross-linked network synthesized in the presence of tripropylene glycol diacrylate (TPGDA) are given in Figure 2d. These curves confirm the expected tendencies of enhanced miscibility gap with increasing  $M_w$  and the neat difference between linear and cross-linked polymers. Since E7 and 5CB have widely different transition temperatures, it is clear that they should cover different domains in the phase diagram. While E7 offers a large temperature window extending from 213 K ( $T_g$ ) to 333 K ( $T_{NI}$ ) with no other transitions in between, 5CB exhibits a nematic transition at 308 K and crystallizes at 296 K. Because of a lack of space, neither the results for E7 nor those involving PMPS will be given here.

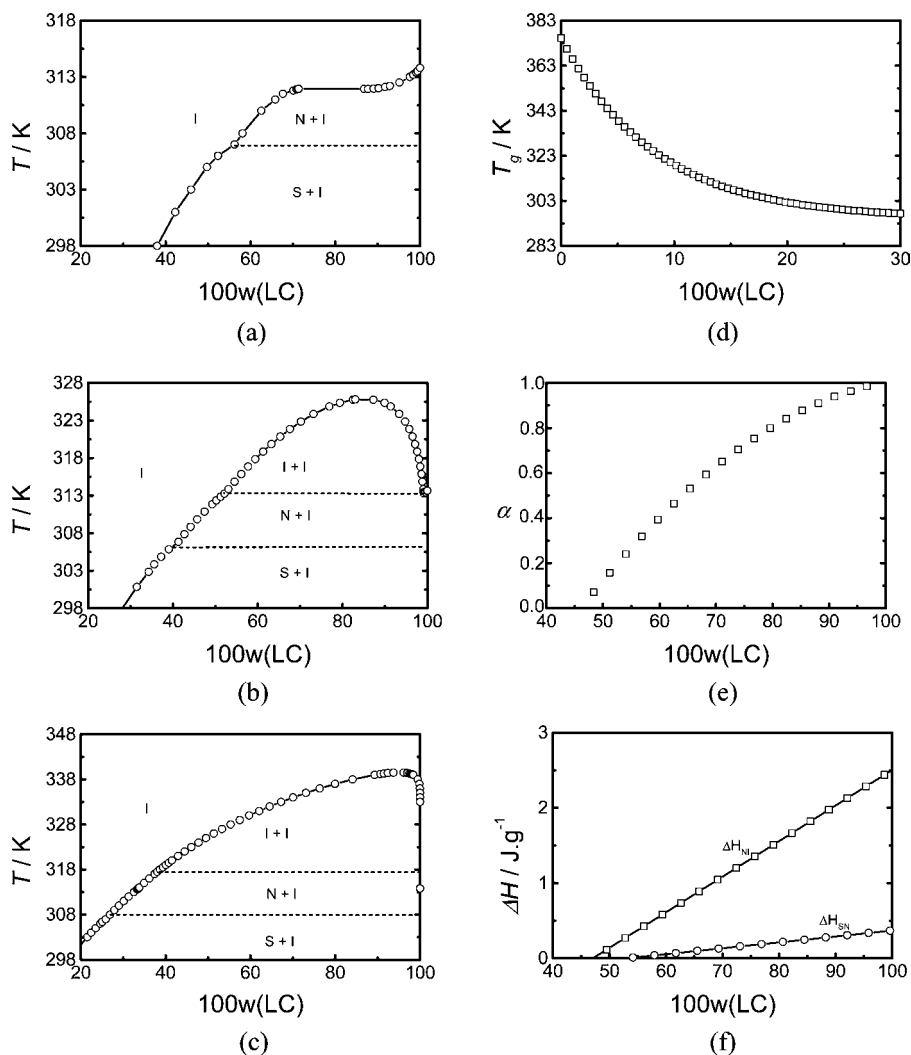


**Figure 1.** (a–c) Phase diagrams of the PS/8CB system for different molecular weights of PS: (a)  $M_w = 4 \text{ kg}\cdot\text{mol}^{-1}$ ,  $N_1 = 1$ ,  $N_2 = 2$ ,  $\chi = -4.558 + (1733.14 \text{ K})/T$ ; (b)  $M_w = 44 \text{ kg}\cdot\text{mol}^{-1}$ ,  $N_1 = 1$ ,  $N_2 = 32$ ,  $\chi = -2.408 + (1010.76 \text{ K})/T$ ; (c)  $M_w = 200 \text{ kg}\cdot\text{mol}^{-1}$ ,  $N_1 = 1$ ,  $N_2 = 361$ ,  $\chi = -4.558 + (1733.14 \text{ K})/T$ . The transition temperatures characterizing 8CB are  $T_{SN} = 306.5 \text{ K}$  and  $T_{NI} = 313.5 \text{ K}$ , and the interaction parameter for smectic order is  $\zeta = 0.9375$ . I, N, and S denote the isotropic, nematic, and smectic-A phases, respectively. (d)  $T_g$  vs LC mass fraction  $w(\text{LC})$  for the PS/8CB system. (e) Fractional amount of LC segregated ( $\alpha$ ) vs  $w(\text{LC})$ . (f)  $\Delta H_{NI}$  and  $\Delta H_{SN}$  vs  $w(\text{LC})$ . In all of the diagrams presented here,  $N_1$ ,  $N_2$ , and  $\chi$  are fit parameters in the theory.

**Polyacrylates.** Table 1 gives a list of some acrylates with different functionalities. Monofunctional monomers yield linear polymers, while di- and trifunctional ones yield cross-linked networks.

The phase diagram of poly(*n*-butyl acrylate) and E7 reported in ref 32 exhibited a certain anomaly between  $w(\text{E7}) = 0.40$  and  $w(\text{E7}) = 0.80$  that was attributed to a phase separation of the E7 eutectic mixture and preferential solvation of some of its components to poly(*n*-butyl acrylate). A detailed analysis of the morphology and distribution of droplets throughout the phase diagram was reported in this reference, showing that the mean diameter of the droplets increased linearly with  $w(\text{LC})$ .

A similar investigation using poly(ethylhexyl acrylate) (PEHA) and E7 was reported in ref 33. In this case, the polymerization was implemented by UV exposure in the presence of an initiator (Darocur). Both monomeric and polymerized samples were investigated in ref 33, and Figure 3 reproduces some results. Figure 3a shows the diagram of UV-cured PEHA/E7, while (b) shows  $\Delta H_{NI}$  as a function of  $w(\text{LC})$ . In comparison, the case of the difunctional monomer 1,6-hexanediol diacrylate (HDDA) was investigated in ref 34 and requires some attention here. Polymerization was implemented under UV curing in the presence of Darocur, and the results shown in Figure 4a indicate

a typical behavior for cross-linked networks. As the solvent uptake reaches an upper limit, any excess forms a pure phase. This is typical behavior that yields an upturn in the curve above  $T_{NI}$ . In order to improve the data fit, the rubberlike elasticity parameters  $\alpha$  and  $\beta$  should be treated as functions of monomer functionality and LC mass fraction. Figure 4b gives  $\Delta H_{NI}$  and  $\Delta C_p$  as functions of  $w(\text{LC})$ .  $\Delta H_{NI}$  for the monomer system is smaller than that for the cured system, and the  $\Delta C_p$  curve predicts a lower limit of LC solubility. Figure 4c shows that the amount of segregated LC is different depending on whether one considers  $\Delta C_p$  or  $\Delta H_{NI}$ , confirming the fact that  $\Delta C_p$  yields systematically higher  $\alpha$  values than  $\Delta H_{NI}$ .

The trifunctional acrylate glycol propyl triacrylate (GPTA) was also investigated along the same lines, including monomer and cured systems with 5CB, 8CB, and E7 (Figure S11 in the Supporting Information).<sup>35–37</sup> The phase properties involved a variety of textures exhibiting nematic and smectic-A orders in addition to liquid–liquid miscibility gaps. Samples with GPTA were exposed to electron beam irradiation, a technique known to be highly efficient, especially in avoiding the use of an initiator to trigger the polymerization process.

**Norland Optical Adhesive 65.** Unlike the examples above, the following results for Norland Optical Adhesive 65 (NOA65)

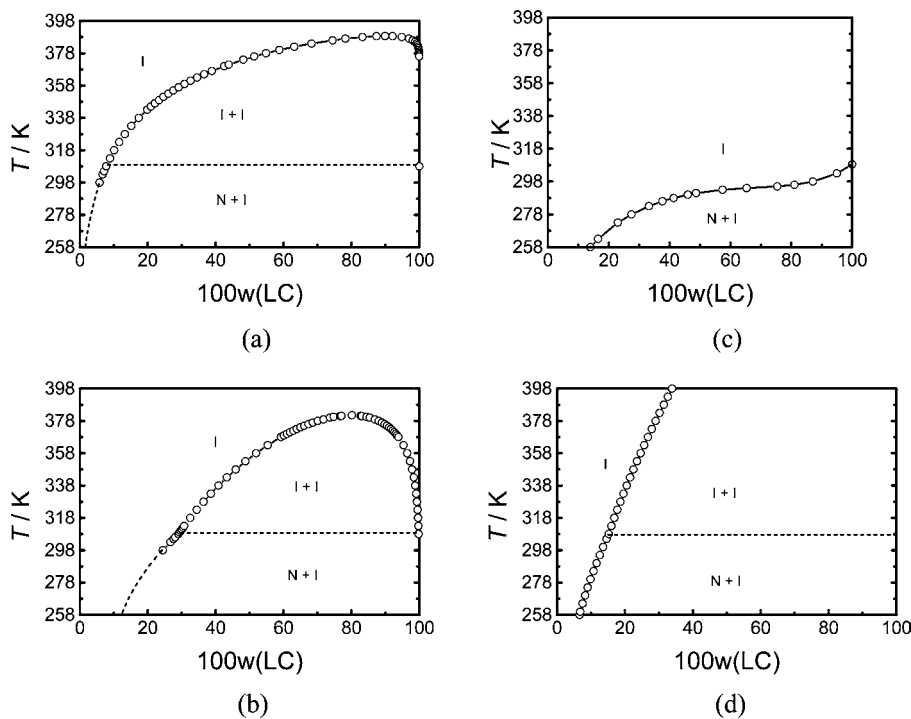


**Figure 2.** (a–c) Phase diagrams of the PDMS/5CB system for different molecular weights of PDMS: (a)  $M_w = 44 \text{ kg}\cdot\text{mol}^{-1}$ ,  $N_1 = 1$ ,  $N_2 = 80$ ,  $\chi = -4.4 + (1950 \text{ K})/T$ ; (b)  $M_w = 5.5 \text{ kg}\cdot\text{mol}^{-1}$ ,  $N_1 = 1$ ,  $N_2 = 16$ ,  $\chi = -0.7 + (565 \text{ K})/T$ ; (c)  $M_w = 0.8 \text{ kg}\cdot\text{mol}^{-1}$ ,  $N_1 = 1$ ,  $N_2 = 5$ ,  $\chi = -2.65 + (1073 \text{ K})/T$ . (d) Phase diagram for a PDMS network cross-linked with TPGDA:  $N_1 = 1$ ,  $N_c = 5$ ,  $\chi = -0.87 + (687 \text{ K})/T$ ,  $\alpha = (f - 2 + 2\phi_2)/f$ ,  $\beta = 2\phi_2/f$ ,  $f = 3$ . The transition temperature for 5CB is 308.3 K.

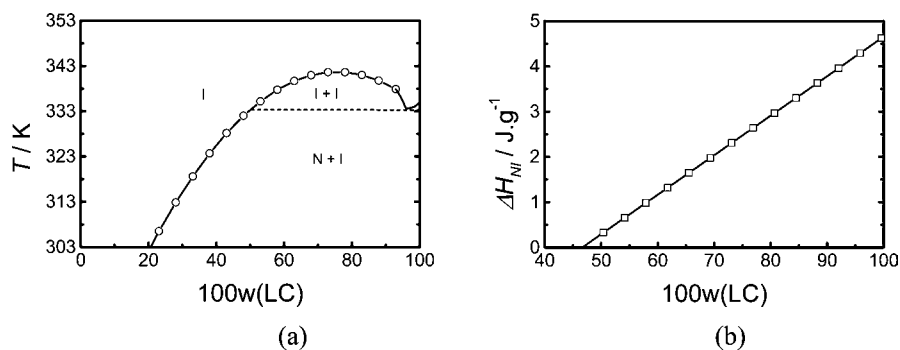


**Figure 3.** (a) Phase diagram of the PEHA/E7 system:  $M_w = 108 \text{ kg}\cdot\text{mol}^{-1}$ ;  $N_1 = 1$ ,  $N_2 = 16$ ,  $\chi = -2.49 + (1123 \text{ K})/T$ . (b)  $\Delta H_{NI}$  vs  $w(\text{LC})$  for the same system. The intersection with the  $x$  axis yields the limit of solubility.

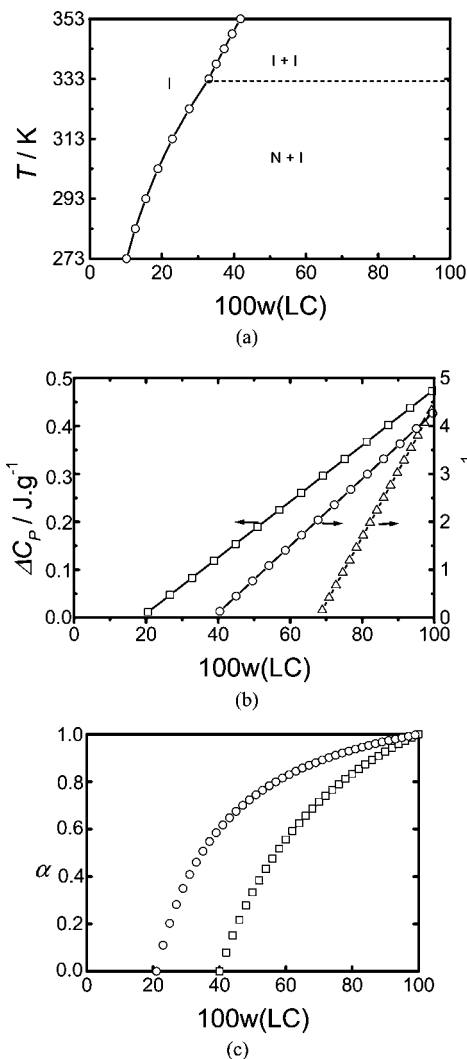
have not been previously reported in the literature and will be presented here in greater detail. First, we note that NOA is a commercial system whose composition is protected and only partially disclosed in the literature. It contains trimethylolpropane diallyl ether, trimethylolpropane trithiol, and isophorone diisocyanate ester, and the mass fraction of benzophenone photoinitiator is  $w = 0.05$ .<sup>38,39</sup> It has mercaptan dopants used in many adhesives and shows excellent adhesion and ability to cure epoxies rapidly under ambient conditions with very low toxicity in comparison with ordinary hardeners. In this work, we used the specific product NOA65, which is characterized by a glass transition at  $T_g(\text{NOA65}) = 213 \text{ K}$ . The properties of NOA65 and E7 compounds were studied before and after exposure to a laser beam in an effort to establish correlations between the conditions of preparation and thermophysical behavior (see section SI2 in the Supporting Information).

Figure 5 shows the phase diagram of the monomeric NOA65/E7 system. Symbols represent experimental data obtained by DSC (○) and confirmed by POM (△); the solid line was obtained from theoretical modeling using the formalism presented in Theoretical Considerations. Essentially two distinct

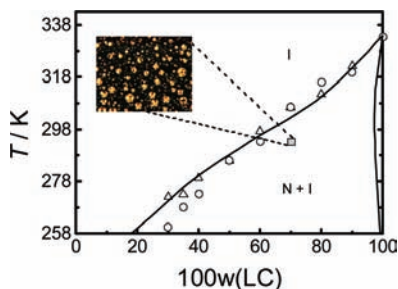
regions can be identified: On the left-hand side of the solid line, the system presents a homogeneous isotropic state. On the right-hand side, the system shows a gap of miscibility wherein a monomer-rich liquid is in equilibrium with a nematic phase. A typical practical situation at ambient temperature and  $w(\text{E7}) = 0.70$  is indicated by the small square in Figure 5, where the system exhibits the morphology shown in the inset. This phase behavior corresponds to a real situation encountered in comutable windows and controlled-light-transmission devices.

Figure 6 shows several of the DSC thermograms used to obtain the ○ data in Figure 5. These thermograms cover the full range of compositions, including pure NOA65. The top curve [ $w(\text{E7}) = 0.90$ ] exhibits two peaks corresponding to the  $N \rightarrow I$  transition near 323 K and the glass transition near 213 K. Upon addition of monomer NOA65, the NI transition shifts to lower temperatures. The peak area yields the amount of heat exchange at the transition for different compositions, providing key information on the miscibility limit and the amount of segregated LC.

The Flory–Huggins interaction parameter used to calculate the phase diagram is plotted against  $T^{-1}$  in Figure 7 for both



**Figure 4.** (a) Phase diagram of the UV-cured HDDA/E7 system:  $N_1 = 1$ ,  $N_c = 5$ ,  $\chi = -1.6 + (823 \text{ K})/T$ ,  $\alpha = (f - 2 + 2\varphi_2)/f$ ,  $\beta = 2\varphi_2/f$ ,  $f = 3$ . The upturn above  $T_{NI}$  is characteristic of a cross-linked network. Reference 34 shows certain discrepancies with the experimental data above  $T_{NI} = 333 \text{ K}$  for reasons that remain to be elucidated. (b)  $\Delta C_p$  (top curve) and  $\Delta H_{NI}$  (middle curve) vs  $w(LC)$  for the UV-cured HDDA/E7 system. The bottom curve is  $\Delta H_{NI}$  vs  $w(LC)$  for uncured HDDA/E7. (c) Amount of segregated LC ( $\alpha$ ) vs  $w(LC)$ . The upper curve was obtained from  $\Delta C_p$  and the lower one from  $\Delta H_{NI}$ .



**Figure 5.** The phase diagram of monomer NOA65/E7 system. Triangles represent POM data ( $\Delta$ ) and circles DSC data ( $\circ$ ). The solid line is a theoretical modeling. I means isotropic and N nematic. The square inside diagram corresponds to a particular situation with  $T = 293 \text{ K}$  and  $w(E7) = 0.70$ . The micrograph shows the morphology under this situation.

the monomer and polymer systems. The decrease in  $\chi$  upon heating is much steeper in the polymer case. Both lines tend to meet in the high-temperature range, but the polymer remains much less compatible with the LC.

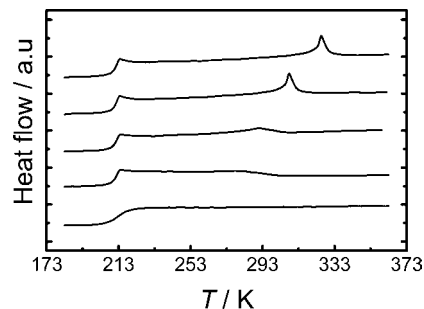


**Figure 6.** DSC thermograms giving heat flow (in arbitrary units) vs temperature for the monomer NOA65/E7 system for several LC mass fractions  $w(E7)$  in descending order: 0.90, 0.70, 0.50, 0.30, 0.

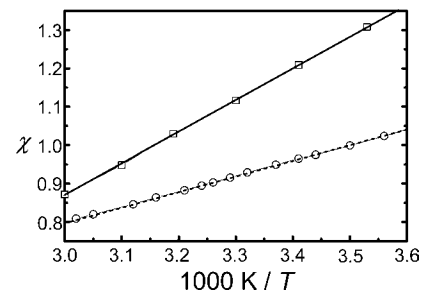


**Figure 7.** Interaction parameter for isotropic mixing ( $\chi$ ) vs  $T^{-1}$  for the polymer (upper line) and monomer (lower line) NOA65/E7 systems.

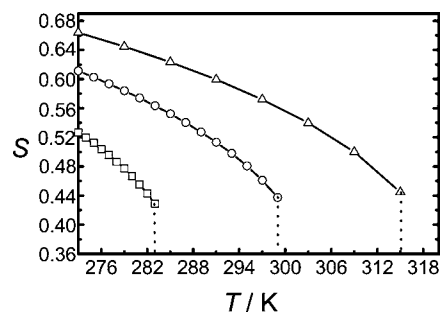


**Figure 8.** Nematic order parameter  $S$  vs temperature for the NOA65/E7 polymer system at three LC mass fractions  $w(E7)$  (0.85, 0.90, and 0.95 from left to right). The sudden decrease in  $S$  to zero indicates a first-order transition from the nematic state to the isotropic state.

A typical temperature profile for a PDLC film would be  $T(x) = T_e + [(T_i - T_e)/L]x$ , where  $L$  is the film thickness and  $T_i$  and  $T_e$  are the temperatures at  $x = L$  and  $x = 0$ , respectively. This profile shows a temperature drop from  $T_0 = 308 \text{ K}$  to  $T_L = 293 \text{ K}$  that influences the electro-optical responses and order parameters for the segregated LC. LC molecules in droplets and in the polymer network would respond differently, since the temperature experienced by molecules located on one side of the film is near  $308 \text{ K}$ , while that for molecules on the other side is near  $293 \text{ K}$ . Therefore, the orientation behavior of LC molecules is not uniform throughout the thickness  $L$ , and this may be quantified by examining the variation of the nematic order parameter with temperature.

It should be noted that the nematic interaction becomes effective only when the LC mass fraction exceeds a certain threshold roughly near  $T/T_{NI}$ , which means that the order parameter  $S$  must exceed a minimum value. These features are illustrated in Figure 8, where the temperature dependence of  $S$  is shown for different LC mass fractions. A sudden decrease in  $S$  takes place at the temperature where the LC mass fraction reaches the threshold, indicating a first-order transition from the nematic state to the isotropic state. This means that

temperature drifts throughout the medium induce modulated responses of LC molecules, which are often ignored in the calculation of phase diagrams. As the temperature increases, more LC molecules diffuse into the polymer matrix, strengthening the plasticizing effect.

## Discussion and Conclusion

This paper has dealt with the thermophysical and phase properties of PDLC systems. These properties have been the subject of particular attention for decades and are still being investigated actively in the literature<sup>40–44</sup> because of the importance of PDLCs from the fundamental point of view and the large prospects for their novel application in modern technologies.

The theoretical framework reported here was developed to rationalize experimental data in a simple and effective way. It allows one to analyze quite successfully the phase behavior and thermophysical properties of PDLC systems. For monomers and linear polymers, the Flory–Huggins lattice model is sufficient to rationalize data in the isotropic state. This theory provides a clear picture with physical parameters that are readily accessible to experimental evaluation. For example, coordinates of the critical point give a relationship between  $N_1$  and  $N_2$ . For LCs, one may reasonably put  $N_1 = 1$  (a single unit), so  $N_2$  can be deduced from  $\varphi_c$ . If the critical point is not well-defined in the phase diagram, then  $N_2$  can be deduced from molar masses or volumes. Only one constant of the critical parameter,  $\chi_c = A + B/T_c$  remains to be determined by data fitting.

In the case of cross-linked networks, the Flory–Rehner theory is used to describe the rubberlike elasticity of the network and the effects of cross-links in inhibiting polymer swelling. In addition to the average number of monomers between consecutive cross-links,  $N_c$ , parameters such as  $\alpha$  and  $\beta$  should be determined to complete the description of polymer elasticity. Flory<sup>5,6</sup> and Petrovic<sup>22</sup> suggested that  $\alpha$  and  $\beta$  should be related to monomer functionality and composition. The problem is somewhat subtle, since the conditions of network preparation and in particular the compositions prior to polymerization have an important impact on the system properties.

With a very large degree of polymerization, entropic contributions are significantly reduced and the network can be viewed as a single molecule. When swelling reaches an upper limit, a pure solvent phase appears, and determination of the composition of the coexisting phases is simplified because a single equation can be solved by equating the polymer chemical potential to zero. In order to improve the accordance between theory and experiment, the interaction parameter is often treated as both temperature- and composition-dependent, unlike the case of linear polymers, where the temperature dependence is normally sufficient.

The nematic-order contribution to the free energy can be modeled according to the Maier–Saupe mean-field theory of thermotropic LCs. Extension of this theory to smectic-A order was implemented by McMillan in a straightforward manner. Concrete examples with 8CB demonstrated the usefulness of the McMillan theory to rationalize experimental findings. Interestingly, a coupling parameter permitted the case of a direct transition from isotropic to smectic-A order as well as a succession of transitions from isotropic to nematic to smectic phases to be treated. For nematogen mixtures, the strength of coupling governs the departure from pure LC properties, and higher-order smectic-A structures may be induced, as explained by Kyu and co-workers.<sup>45</sup>

A variety of thermophysical properties have also been considered in addition to the phase diagrams. LC molecules

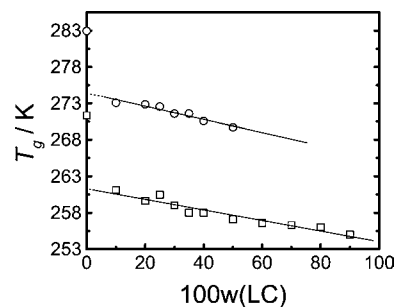


**Figure 9.**  $T_g$  vs  $w(\text{LC})$  for the NOA65/E7 system obtained using DSC (○) and mechanical measurements (□).

dispersed in the polymer lead to a drop in  $T_g$  and plasticizing effects that have important implications for mechanical strength, polymer aging, and other properties, including optical and dielectric properties. In order to quantify these effects, the amount of segregated LC in droplets must be determined and the conditions of segregation must be controlled. The analysis can be implemented using either the heat exchange at the transition or the thermal capacity  $\Delta C_p$ . The qualitative tendencies obtained from these two analyses are consistent, but quantitative discrepancies do exist (e.g., Figure 4b).

Likewise, the glass transition temperature can be deduced either from DSC or mechanical data. While the calorimetric method is in principle more appropriate for a thermodynamic property such as  $T_g$ , it is always useful to validate the results by other means, such as a thermomechanical technique. An example of this comparison is given in Figure 9. Both techniques predict a linear decrease in  $T_g$  upon dilatation by the LC, but the thermomechanical data underestimate  $T_g$  systematically over the whole range of LC mass fraction.<sup>46</sup>

The problem of cross-linked networks raises a variety of questions distinct from those of linear-chain systems. The cross-links oppose swelling beyond a certain limit, leading to a pure solvent phase. Hence, the theoretical analysis requires a model of rubberlike elasticity with additional physical parameters. A higher cross-linking density yields a tougher network, which is expressed by  $N_c$ , the number of monomers between consecutive cross-links. A larger value of  $N_c$  means a looser network. This parameter can be inferred from mechanical data. On the other hand, the thermophysical properties are different depending on whether polymerization is made in a melt or in solution. Unavoidable heterogeneities in cross-linking lead to different network structures. Highly cross-linked regions swell less than loose ones, further complicating the analysis of the phase behavior. Moreover, the cross-linking density increases with the monomer functionality, and the phase diagrams show larger gaps of miscibility for monomers with higher functionalities and molar masses. Typical examples illustrating these features have been given.

In conclusion, this paper has reviewed the current situation concerning the phase behavior and thermophysical properties of PDLCs. These materials are increasingly important because they open up wide areas of applications in a variety of modern technologies, including communication systems and display devices. Both initial mixtures and cured systems have been considered in order to see the impact of curing on the properties. Because of a lack of space, time evolutions between initial and final states have been omitted. Such a study would have required detailed analyses of the kinetics of polymerization/cross-linking and phase separation that are beyond the scope of the present work. For the same reason, we have omitted discussion of electro-optical properties, which are the basis for most applications of PDLCs. For more details on these issues, the reader is referred to refs 47 and 48.



## Acknowledgment

We thank all of our friends and colleagues from Lille and Dunkerque (France) and Mainz (Germany) with whom we shared years of fruitful collaboration in a very good spirit. We especially thank Dr. U. Maschke and Profs. X. Coqueret, J.-M. Buisine, A. Daoudi, A. Hadj Sahraoui, and F. Roussel.

## Supporting Information Available:

Results for GPTA/LC composites and the NOA65/E7 system. This material is available free of charge via the Internet at <http://pubs.acs.org>.

## Literature Cited

- de Gennes, P. G.; Prost, J. *The Physics of Liquid Crystals*; Oxford University Press: Oxford, U.K., 1994.
- Chandrasekhar, S. *Liquid Crystals*, 2nd ed.; Cambridge University Press: Cambridge, U.K., 1992.
- Doane, J. W. *Polymer Dispersed Liquid Crystal Displays*; World Scientific: Singapore, 1990.
- Drzaic, P. S. *Liquid Crystal Dispersions*; World Scientific: Singapore, 1995.
- Flory, P. J. *Principles of Polymer Chemistry*; Ithaca Press: New York, 1956.
- Flory, P. J.; Rehner, J. Thermodynamics of heterogeneous polymers and their solutions. *J. Chem. Phys.* **1944**, *12*, 425–438.
- Brochard, F.; Jouffroy, J.; Levinson, P. Phase diagrams of mesomorphic mixtures. *J. Phys. (Paris)* **1984**, *45*, 1125–1136.
- McMillan, W. L. Simple Molecular Model for the Smectic A Phase of Liquid Crystals. *Phys. Rev. A* **1971**, *4*, 1238–1246.
- Hino, T.; Prausnitz, J. M. A perturbed hard-sphere-chain equation of state for nematic liquid crystals and their mixtures with polymers. *Liq. Cryst.* **1997**, *22*, 317–326.
- Abe, A.; Ballauff, M. *The Flory Lattice Model*; World Scientific: Singapore, 1992.
- Orendi, H.; Ballauff, M. Complete phase diagrams of mixtures of a nematic liquid crystal with *n*-alkanes. *Liq. Cryst.* **1989**, *6*, 497–500.
- Ballauff, M. Phase diagrams of mixtures of liquid crystals and polymers: Nematic–isotropic phase equilibria versus liquid–liquid demixing. *Mol. Cryst. Liq. Cryst. Lett.* **1986**, *4*, 15–22.
- Ballauff, M. Swelling Equilibria of Networks in Nematogenic Solvents. *Mol. Cryst. Liq. Cryst.* **1991**, *196*, 47–55.
- Shen, C.; Kyu, T. Spinodals in a polymer dispersed liquid crystal. *J. Chem. Phys.* **1995**, *102*, 556–562.
- Nwabunma, D.; Kyu, T. Phase Behavior of Mixtures of Low Molar Mass Nematic Liquid Crystal and in Situ Photo-Cross-Linked Polymer Network. *Macromolecules* **1999**, *32*, 664–674.
- Nwabunma, D.; Kim, K. J.; Lin, Y.; Chien, L. C.; Kyu, T. Phase Diagram and Photopolymerization Behavior of Mixtures of Uv-Curable Multifunctional Monomer and Low Molar Mass Nematic Liquid Crystal. *Macromolecules* **1998**, *31*, 6806–6812.
- Benmouna, F.; Coqueret, X.; Maschke, U.; Benmouna, M. Phase Behavior of Blends of Polymers and Smectic-A Liquid Crystals. *Macromolecules* **1998**, *31*, 4879–4890.
- Benmouna, F.; Bedjaoui, L.; Maschke, U.; Coqueret, X.; Benmouna, M. On the phase behavior of blends of polymers and nematic liquid crystals. *Macromol. Theory Simul.* **1998**, *7*, 599–611.
- Benmouna, F.; Maschke, U.; Coqueret, X.; Benmouna, M. Equilibrium phase behavior of polymer and liquid crystal blends. *Macromol. Theory Simul.* **2000**, *9*, 215–229.
- James, H.; Guth, E. J. Theory of the Increase in Rigidity of Rubber during Cure. *J. Chem. Phys.* **1947**, *15*, 669–683.
- Queslel, J. P.; Mark, J. E. Swelling Equilibrium Studies of Elastomeric Network Structures. *Adv. Polym. Sci.* **1985**, *71*, 230–247.
- Petrovic, Z. S.; MacKnight, W. J.; Koningsveld, R.; Dusek, K. Swelling of Model Networks. *Macromolecules* **1987**, *20*, 1088–1096.
- Blumstein, A.; Hsu, E. C. In *Liquid Crystalline Order in Polymers*; Blumstein, A., Ed.; Academic Press: New York, 1978.
- Polymer Liquid Crystals*; Ciferri, A., Kyhan, W. R., Meyer, R. B., Eds.; Academic Press: New York, 1983.
- Chiu, H. W.; Kyu, T. Equilibrium phase behavior of nematic mixtures. *J. Chem. Phys.* **1995**, *103*, 7471–7481.
- Benmouna, F.; Daoudi, A.; Roussel, F.; Buisine, J.-M.; Coqueret, X.; Maschke, U. Equilibrium Phase Diagram of Polystyrene and 8CB. *J. Polym. Sci., Part B: Polym. Phys.* **1999**, *37*, 1841–1848.
- Maschke, U.; Daoudi, A.; Roussel, F.; Buisine, J.-M.; Coqueret, X.; Benmouna, M. Equilibrium Phase Properties of Polymer/Liquid Crystal Blends: Theory and Experiments. *Mol. Cryst. Liq. Cryst.* **2001**, *365*, 405–413.
- Maschke, U.; Gogibus, N.; Noirez, L.; Ewen, B.; Wagner, T.; Benmouna, M. Liquid Crystal 8CB/Deuterated Polystyrene: Investigations by Small Angle Neutron Scattering. *Mol. Cryst. Liq. Cryst.* **2001**, *367*, 259–266.
- Gogibus, N.; Maschke, U.; Benmouna, F.; Ewen, B.; Coqueret, X.; Benmouna, M. Thermo-Optical Investigations of Polysiloxane/Liquid Crystal Mixtures. *Mol. Cryst. Liq. Cryst.* **2001**, *365*, 675–683.
- Gogibus, N.; Maschke, U.; Benmouna, F.; Roussel, F.; Ewen, B.; Coqueret, X.; Buisine, J.-M.; Benmouna, M. Effects of Polymer Architecture on the Phase Properties of Polymethylsiloxane/Liquid Crystal Blends. *Mol. Cryst. Liq. Cryst.* **2001**, *365*, 665–673.
- Gogibus, N. Etudes des propriétés thermophysiques et électro-optiques de mélanges de polysiloxanes et de cristaux liquides. Ph.D. Thesis, University of Lille, Lille, France, 2001.
- Bouchaour, T.; Benmouna, F.; Leclercq, L.; Ewen, B.; Coqueret, X.; Benmouna, M.; Maschke, U. Phase equilibrium of poly(*n*-butyl acrylate) and E7. *Liq. Cryst.* **2000**, *27*, 413–420.
- Roussel, F.; Buisine, J.-M.; Maschke, U.; Coqueret, X.; Benmouna, F. *Phys. Rev. E* **2000**, *62*, 541–548.
- Roussel, F.; Maschke, U.; Buisine, J.-M.; Coqueret, X.; Benmouna, F. Phase Properties of Hexanediol diacrylate/E7 Blends. *Mol. Cryst. Liq. Cryst.* **2001**, *365*, 685–693.
- Maschke, U.; Benmouna, F.; Roussel, F.; Daoudi, A.; Gyselinck, F.; Buisine, J.-M.; Coqueret, X.; Benmouna, M. Phase Diagrams of Monomeric and Electron Beam Cured Propoxylylated Glyceroltriacylate/Low Molecular Weight Liquid Crystal Systems. *Mol. Cryst. Liq. Cryst.* **2001**, *365*, 655–663.
- Maschke, U.; Roussel, F.; Daoudi, A.; Gyselinck, F.; Buisine, J.-M.; Coqueret, X.; Benmouna, M. *Polym. Bull.* **2000**, *44*, 577.
- Maschke, U.; Benmouna, F.; Roussel, F.; Daoudi, A.; Gyselinck, F.; Buisine, J.-M.; Coqueret, X.; Benmouna, M. Phase behavior of electron beam cured and uncured propoxylylated glyceroltriacylate/E7 mixtures. *Polym. Bull.* **2000**, *44*, 577–584.
- Smith, G. W. Cure Parameters and Phase Behavior of an Ultraviolet-Cured Polymer-Dispersed Liquid Crystal. *Mol. Cryst. Liq. Cryst.* **1991**, *196*, 89–102.
- Senyurt, A. F.; Warren, G.; Whitehead, J. B., Jr.; Hoyle, C. E. Matrix physical structure effect on the electro-optic characteristics of thiol–ene based H-PDLC films. *Polymer* **2006**, *47*, 2741–2749.
- Soulé, E. R.; Abukhdeir, N. M.; Rey, A. D. Thermodynamics, Transition Dynamics, and Texturing in Polymer Dispersed Liquid Crystals with Mesogens Exhibiting a Direct Isotropic/Smectic-A Transition. *Macromolecules* **2009**, *42*, 9486–9497.
- Kim, N.; Choi, J.; Chien, L.-C.; Kyu, T. Phase Equilibria of a Mixture of Side-Chain Liquid Crystalline Polymer and Low Molecular Weight Liquid Crystal. *Macromolecules* **2007**, *40*, 9582–9589.
- Meng, S.; Duran, H.; Hu, J.; Kyu, T.; Natarajan, L. V.; Tondiglia, V. P.; Sutherland, R. L.; Bunning, T. J. Influence of Photopolymerization Reaction Kinetics on Diffraction Efficiency of H-PDLC Undergoing Photopatterning Reaction in Mixtures of Acrylic Monomer/Nematic Liquid Crystals. *Macromolecules* **2007**, *40*, 3190–3197.
- Xia, J.; Wang, J.; Lim, Z.; Qiu, F.; Yang, Y. Phase Separation of PDLC Confined between Two Parallel Walls. *Macromolecules* **2006**, *39*, 2247–2253.
- White, T. J.; Natarajan, L. V.; Tondiglia, V. P.; Bunning, T. J.; Guyman, C. A. Polymerization Kinetics and Monomer Functionality Effects in Thiol–Ene PDLCs. *Macromolecules* **2007**, *40*, 1112–1120.
- Kyu, T.; Liang, S.; Chiu, H.-W. Phase Diagrams and Evolution of Mesophase Structure in Mixtures of a Low Molar Mass Smectic Liquid Crystal and a Nematic Side-on Side-Chain Liquid Crystalline Polymer. *Macromolecules* **1998**, *31*, 3604–3611.
- Benmouna, R.; Benyoucef, B. Thermophysical and Thermomechanical Properties of Norland Optical Adhesives and Liquid Crystal Composites. *J. Appl. Polym. Sci.* **2008**, *108*, 4072–4079.
- Benmouna, R.; Coqueret, X.; Maschke, U.; Bouchaour, T.; Rachet, V.; le Barny, P.; Feneyrou, P. Investigation of Polymer Dispersed Liquid Crystal Films Exhibiting Nanosized Liquid Crystalline Domains. *Mol. Cryst. Liq. Cryst.* **2004**, *422*, 135–141.
- Benmouna, R.; Rachet, V.; le Barny, P.; Feneyrou, P.; Maschke, U.; Coqueret, X. FTIR and UV-Visible Spectroscopy Studies of Thiolene/E7 Composites Showing Nanodispersion: Curing Kinetics and Electro-Optical Properties. *J. Polym. Eng.* **2006**, *26*, 499–510.

Received for review October 19, 2009. Accepted March 9, 2010.

JE9008552